

Epigraph-Guided Flow Matching for Safe and Performant Offline Reinforcement Learning

Manan Tayal ^{*1} Mumuksh Tayal ^{*1}

Abstract

Offline reinforcement learning (RL) provides a compelling paradigm for training autonomous systems without the risks of online exploration, particularly in safety-critical domains. However, jointly achieving strong safety and performance from fixed datasets remains challenging. Existing safe offline RL methods often rely on soft constraints that allow violations, introduce excessive conservatism, or struggle to balance safety, reward optimization, and adherence to the data distribution. To address this, we propose Epigraph-Guided Flow Matching (EpiFlow), a framework that formulates safe offline RL as a state-constrained optimal control problem to co-optimize safety and performance. We learn a feasibility value function derived from an epigraph reformulation of the optimal control problem, thereby avoiding the decoupled objectives or post-hoc filtering common in prior work. Policies are synthesized by reweighting the behavior distribution based on this epigraph value function and fitting a generative policy via flow matching, enabling efficient, distribution-consistent sampling. Across various safety-critical tasks, including Safety-Gymnasium benchmarks, EpiFlow achieves competitive returns with near-zero empirical safety violations, demonstrating the effectiveness of epigraph-guided policy synthesis.

1. Introduction

Autonomous systems are increasingly deployed in safety-critical domains such as self-driving vehicles (Kiran et al., 2021), robotics, aerospace, and healthcare (Gottesman et al., 2019). Designing control algorithms for these systems requires balancing two competing objectives: achieving high task performance under practical constraints while ensuring

safety to prevent severe failures. These objectives are inherently in tension, as aggressively optimizing performance can increase the risk of unsafe behavior.

Reinforcement learning (RL) (Sutton et al., 1999) has emerged as a powerful framework for learning complex control policies directly from interaction data. However, in safety-critical settings, unrestricted online exploration can be prohibitively risky. Constrained reinforcement learning (CRL) methods seek to incorporate safety requirements into policy optimization, commonly through Lagrangian relaxations or runtime shielding mechanisms (Achiam et al., 2017; Altman, 2021; Alshiekh et al., 2018; Zhao et al., 2023). While effective in simulated environments, most CRL approaches rely on extensive online interaction, which is often impractical for real systems due to safety concerns or the absence of accurate simulators (Liu et al., 2024b). These challenges have spurred growing interest in offline RL and imitation learning, where policies are learned solely from pre-collected datasets (Kumar et al., 2020). By eliminating the need for online exploration, offline RL (Levine et al., 2020) provides a promising pathway for deploying learning-based controllers in safety-critical domains.

Despite this promise, achieving reliable safety in offline RL remains difficult. Many existing safe offline RL methods enforce safety through expected cumulative costs or penalties (Xu et al., 2022; Stooke et al., 2020), effectively treating safety as a soft constraint. Such formulations allow non-zero violation risk and are therefore unsuitable for applications that require state-wise safety guarantees, where even a single violation is unacceptable. Moreover, jointly optimizing performance and safety from static datasets often leads to unstable learning dynamics or overly conservative policies, particularly when unsafe transitions are rare or entirely absent from the data (Lee et al., 2022).

A more rigorous alternative arises from classical optimal control, where safety and performance are jointly addressed by formulating the problem as a *state-constrained optimal control problem* (SC-OCP). In this setting, safety is encoded as a hard state constraint, while performance is captured through a reward or cost functional. Despite its strong theoretical foundations, solving SC-OCPs in practice is difficult: the existence and characterization of optimal so-

^{*}Equal contribution ¹TAU Intelligence. Correspondence to: Manan Tayal <tayalmanan28@gmail.com>.

lutions typically rely on stringent controllability conditions (Soner, 1986). To mitigate these difficulties, (Altarovici et al., 2013) introduced an epigraph-based reformulation that characterizes the SC-OCP value function by computing its epigraph through dynamic programming, leading to a Hamilton–Jacobi–Bellman (HJB) partial differential equation. The original value function and the associated optimal policy can then be recovered from this epigraph representation. Nevertheless, dynamic programming methods are fundamentally limited by the curse of dimensionality, rendering them impractical for high-dimensional systems when using conventional numerical solvers (Mitchell, 2004; Wang et al., 2024). The epigraph reformulation further augments the state space, compounding the computational burden and limiting applicability to low-dimensional settings. Although various approximation and acceleration strategies have been proposed, they often require restrictive assumptions on system structure or dynamics (Chow et al., 2017b). Consequently, computing solutions to the resulting HJB equations for general nonlinear, high-dimensional control systems remains an open and challenging problem.

In this work, we bridge the gap between rigorous state-constrained control and scalable offline RL by introducing *Epigraph-Guided Flow Matching* (*EpiFlow*). We circumvent the need for solving high-dimensional HJB-PDEs by deriving a data-driven, Bellman-style recursion for an auxiliary epigraph value function. This function acts as a feasibility-aware value function, capturing the maximum achievable performance threshold that remains compatible with future safety. By learning this function directly from transitions, we enable the agent to reason about long-horizon safety and performance without explicit knowledge of the system dynamics. To extract executable policies, we leverage Flow Matching as a scalable generative representation. Unlike diffusion-based policies that require expensive iterative sampling, Flow Matching enables efficient policy synthesis via a single deterministic ODE integration. Our framework guides this generative process using the learned epigraph value function, ensuring that synthesized actions remain strictly within the safe support of the offline distribution while maximizing return. Our approach targets high-confidence feasibility grounded in the data distribution, providing an empirical yet robust safety certificate for deployment in complex environments.

We evaluate the proposed approach across a range of safety-critical benchmarks, including low-dimensional navigation tasks and high-dimensional Safety Gymnasium environments (Ji et al., 2023). Our results show that epigraph-guided synthesis achieves competitive returns with near-zero empirical safety violations, significantly outperforming existing dual-objective and filter-based baselines.

The main contributions of this work are:

- We propose *Epigraph-guided Flow Matching* (*EpiFlow*), a framework which casts safe offline RL as a state-constrained optimal control problem, providing a principled path to co-optimize performance and hard safety constraints.
- We derive a Bellman-style recursion for an auxiliary epigraph value function, enabling the characterization of safe performance envelopes directly from offline data without solving intractable HJB-PDEs.
- We propose a weighted Flow Matching objective that guides generative policy learning toward safe, high-performing regions of the data distribution, ensuring efficient and distribution-consistent sampling in continuous action spaces.
- We demonstrate the effectiveness of *EpiFlow*, across a wide range of safety-critical benchmarks, including high-dimensional Safety Gymnasium tasks, showing near-zero safety violations while maintaining high task returns compared to state-of-the-art safe offline RL methods.

2. Related Works

Safe Offline Reinforcement Learning. Safe reinforcement learning has traditionally been studied in the online setting using Lagrangian-based constrained optimization or trust-region methods (Chow et al., 2017a; Tessler et al., 2018; Stooke et al., 2020; Achiam et al., 2017). These approaches regulate safety through soft cost penalties and typically require online interaction, motivating a shift toward safe offline reinforcement learning. Early offline methods such as CPQ penalize unsafe or out-of-distribution actions (Xu et al., 2022), but this can distort value estimates and hinder generalization (Li et al., 2023). Distribution-matching approaches such as COptiDICE (Lee et al., 2022), building on DICE objectives (Lee et al., 2021), frame constrained policy optimization through stationary distribution correction, but inherit instability and sensitivity associated with residual-gradient learning (Baird, 1995). More broadly, several offline RL methods mitigate extrapolation by constraining policies to remain close to the behavior distribution, including advantage-weighted and distribution-constrained approaches (Peng et al., 2019; Nair et al., 2021; Kumar et al., 2019; Kostrikov et al., 2022). Overall, existing safe offline RL methods often rely on soft constraints or dual optimization and struggle to balance safety and performance when unsafe transitions are sparse.

Safe Generative Policies. Recent work has explored generative policy representations for offline RL, including sequence models and diffusion-based policies (Chen et al., 2021; Janner et al., 2022), with extensions to safety-constrained settings (Liu et al., 2023; Lin et al., 2023; Zheng

et al., 2024; Liu et al., 2025). While effective, diffusion-based policies require simulating stochastic processes over many discretized time steps at inference, which can be computationally expensive and challenging to deploy in control loops. In contrast, flow matching (Lipman et al., 2023; Zhang et al., 2025; Alles et al., 2025) provides a deterministic alternative that directly learns the vector field of the generative process, enabling efficient policy sampling via a single ODE integration.

3. Background and Problem Setup

We study safe offline reinforcement learning in environments with hard state constraints. The environment is modelled as a state-constrained Markov Decision Process (SC-MDP), defined by the tuple $\mathcal{M} = (\mathcal{X}, \mathcal{A}, f, r, \ell, \gamma)$, where \mathcal{X} and \mathcal{A} denote the state and action spaces, $x_{t+1} = f(x_t, a_t)$ denotes an unknown, deterministic transition function, $r : \mathcal{X} \rightarrow \mathbb{R}$ is the reward function, $\ell : \mathcal{X} \rightarrow \mathbb{R}$ is an instantaneous state-based safety function, and $\gamma \in (0, 1)$ is the discount factor. We define the *failure set* $\mathcal{F} := \{x \in \mathcal{X} \mid \ell(x) < 0\}$, which represents unsafe states that must be avoided at all times (e.g., collisions or constraint violations). A trajectory is considered safe if it never enters \mathcal{F} . We assume access to an offline dataset $\mathcal{D} = \{(x_t, a_t, r_t, \ell_t, x_{t+1})\}$, collected by an unknown behavior policy, with no further interaction with the environment permitted. A policy $\pi(a \mid x)$ induces trajectories $\tau = (x_0, a_0, x_1, \dots)$ through the transition dynamics.

3.1. State-Constrained Offline Reinforcement Learning

Given an initial state x , the objective is to compute the maximum achievable discounted return subject to strict state safety at all future time steps. This requirement can be formalized through the following *state-constrained value function*:

$$\begin{aligned} V(x) &= \sup_{\pi} \left[\sum_{k=0}^{\infty} \gamma^k r(x_k) \mid x_0 = x \right] \\ \text{s.t. } &x_t \notin \mathcal{F}, \forall t \geq 0. \end{aligned} \quad (1)$$

Unlike formulations based on expected cumulative penalties, (1) encodes a *hard safety requirement*: only policies that admit trajectories remaining entirely outside the failure set are considered feasible. This formulation directly captures safety-critical requirements where even a single violation is unacceptable.

However, directly optimizing (1) in the offline setting is challenging. Feasibility depends on long-horizon future behavior, which cannot be verified using local penalties or one-step constraints. Moreover, offline datasets often underrepresent unsafe transitions, making it difficult to infer whether a given state admits any safe continuation. As

a result, standard offline RL objectives, which optimize expected return, are ill-suited for enforcing state-wise safety constraints.

3.2. Epigraph Reformulation

The state-constrained value function in (1) jointly optimizes performance and safety, which makes it difficult to reason about directly in the offline setting. To expose the structure of this problem, we adopt an epigraph-based reformulation that expresses the original objective as a two-stage optimization.

In the first stage, the state-constrained value function is characterized as the largest performance threshold that is feasible under the safety constraint:

$$V(x) = \sup\{z \in \mathbb{R} \mid \hat{V}(x, z) \geq 0\}. \quad (2)$$

This formulation makes explicit that $V(x)$ represents the maximum achievable return level that is compatible with safety starting from state x .

The second stage defines the auxiliary value function $\hat{V}(x, z)$, which evaluates whether a given performance threshold z is feasible. Specifically, $\hat{V}(x, z)$ is defined as

$$\hat{V}(x_t, z_t) = \sup_{\pi} \min \left\{ \sum_{k=t}^{\infty} \gamma^{k-t} r(x_k) - z_t, \min_{s \geq t} \gamma^{s-t} \ell(x_s) \right\}. \quad (3)$$

A formal derivation of the epigraph reformulation is provided in Appendix A.1. Discounting is applied to the safety term solely to enable a Bellman-style discrete-time recursion (Eq. (5)); since $\gamma \in (0, 1)$ preserves the sign of $\ell(x)$, this does not alter the hard state constraint and serves only as a technical device for dynamic programming (see Appendix A.1).

The auxiliary value $\hat{V}(x, z)$ is non-negative if and only if there exists a policy that both achieves discounted return at least z and remains outside the failure set at all future time steps. As a result, (2) selects the largest performance threshold for which the safety constraint is feasible.

The scalar variable z therefore plays the role of a performance envelope. Values of z smaller than the optimal threshold correspond to conservative but safe behavior, while values larger than this threshold are infeasible and necessarily lead to safety violations.

For discounted infinite-horizon problems, the auxiliary variable admits the discrete-time update

$$z_{t+1} = \frac{z_t - r(x_t)}{\gamma}, \quad (4)$$

which ensures that the augmented state (x_t, z_t) evolves as a Markov process. This interpretation enables learning the

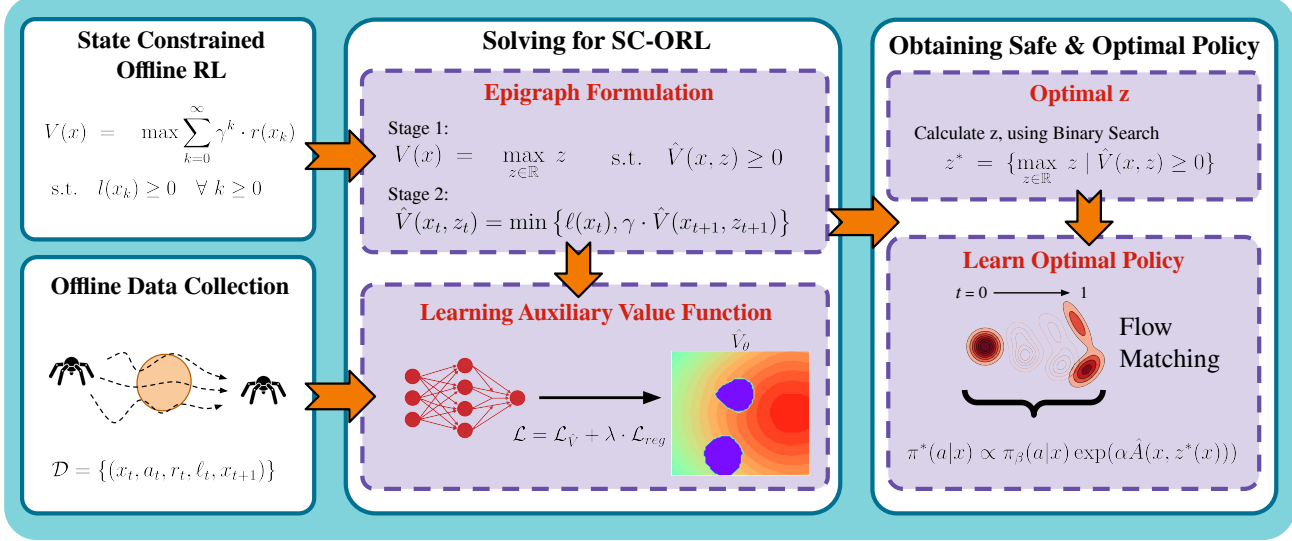


Figure 1. Epiflow Framework. We propose a framework to solve the SC-ORL problem by learning an Auxiliary Value Function, $\hat{V}(x, z)$, using an offline dataset. We formulate an epigraph form for the problem that learns \hat{V} , which if satisfied to stay positive, makes sure that the system stays safe while maximising on the objective. We finally learn a policy which maximises \hat{V} at all time steps to find the most optimal path that the offline data supports.

feasibility structure of $V(x)$ from offline data using value-based methods, without directly enforcing hard constraints during policy optimization.

4. Learning the Epigraph Value Function

In Section 3 we showed that the state-constrained value function $V(x)$ may be characterized via the auxiliary epigraph value function $\hat{V}(x, z)$ through the two-stage formulation (Equations (2),(3)). This section describes a practical, data-driven procedure to learn a dataset-consistent approximation of \hat{V} from offline transitions, and to obtain the state-wise performance envelope $z^*(x)$ used for policy extraction. We first state the recursive form used for learning, then highlight numerical and statistical challenges, and finally present the losses and regularizer we use in practice; implementation-level details are summarized in Algorithm 1 and illustrated in Fig. 1.

4.1. Recursive Characterization

We begin by characterizing the structure of the auxiliary epigraph value function through a Bellman-style recursion.

Theorem 4.1 (Epigraph Value Recursion). *Consider a deterministic SC-MDP with bounded reward and discount factor $\gamma \in (0, 1)$. Given a transition $(x_t, a_t, r_t, \ell_t, x_{t+1})$ and the epigraph update $z_{t+1} = (z_t - r(x_t))/\gamma$, the epigraph value function $\hat{V}(x_t, z_t)$ satisfies the recursion*

$$\hat{V}(x_t, z_t) = \min \{ \ell(x_t), \gamma \hat{V}(x_{t+1}, z_{t+1}) \}. \quad (5)$$

A formal proof is provided in Appendix A.2, and conver-

gence of the recursion can be established using arguments similar to those developed for safety value functions in Hamilton–Jacobi reachability (Fisac et al., 2019).

Although the recursion in (5) provides a principled characterization of epigraph feasibility, directly learning \hat{V} from offline data is ill-conditioned. In particular, the update does not explicitly enforce sensitivity with respect to the epigraph variable z , which causes $\hat{V}(x, z)$ to exhibit weak dependence on z in practice. Empirical evidence in Appendix A.3 shows that the learned \hat{V} profiles are often similar across different values of z , undermining the interpretation of z as a meaningful performance threshold. Moreover, the recursion implicitly involves a supremum over policies, which must be handled carefully in the offline setting to avoid extrapolation beyond the dataset support.

To mitigate the loss of sensitivity to z , we introduce a conservative upper bound derived directly from the epigraph definition:

$$\begin{aligned} \hat{V}(x_t, z_t) &= \sup_{\pi} \min \left\{ \sum_{k=t}^{\infty} \gamma^{k-t} r(x_k) - z_t, \min_{s \geq t} \gamma^{s-t} \ell(x_s) \right\} \\ &\leq \min \left\{ \sup_{\pi} \sum_{k=t}^{\infty} \gamma^{k-t} r(x_k) - z_t, \sup_{\pi} \min_{s \geq t} \gamma^{s-t} \ell(x_s) \right\} \\ &= \min \{ V_r(x_t) - z_t, V_s(x_t) \}, \end{aligned} \quad (6)$$

where, $V_r = \sup_{\pi} \sum_{k=t}^{\infty} \gamma^{k-t} r(x_k)$ and $V_s = \sup_{\pi} \min_{s \geq t} \gamma^{s-t} \ell(x_s)$. This inequality constrains \hat{V} to remain within a feasible range consistent with achievable

performance and safety. This upper bound constrains the scale of \hat{V} and mitigates instability arising from weak conditioning on the epigraph variable z . However, it does not address the statistical challenge posed by the implicit supremum over policies in the epigraph recursion: naïvely replacing this maximization with regression under the behavior policy yields values that reflect behavior-induced feasibility rather than the highest feasible values supported by the dataset.

To handle this issue, we adopt expectile regression (Kostrikov et al., 2022) as a dataset-consistent surrogate for the implicit policy maximization. Expectile regression biases value estimation toward the upper envelope of feasible values supported by the data, without querying out-of-distribution actions, thereby correcting the pessimism induced by behavior-conditioned regression while remaining compatible with offline learning.

Avoiding OOD actions. The epigraph-stage recursion involves a maximization over admissible actions (refer equation (5)) by taking supremum over π . In the offline setting, only behaviour-induced actions are observed, explicit maximization can therefore produce optimistic values corresponding to actions not grounded in the dataset. Expectile regression (Kostrikov et al., 2022) provides a principled surrogate for this maximization: we first fit an action-conditional auxiliary Q-function $\hat{Q}(x, z, a)$ on dataset transitions and then distill an auxiliary state-value $\hat{V}(x, z)$ by minimizing an asymmetric squared loss (expectile) that biases the estimate toward the upper envelope of dataset-supported \hat{Q} values without ever querying unsupported actions. Concretely, the expectile loss $\mathcal{L}^\tau(u) = |\tau - 1(u < 0)|u^2$ with $\tau \in (0.5, 1)$ places greater penalty on underestimation than overestimation. This produces a value \hat{V} that (i) captures high-but-supported values induced by the behaviour policy, and (ii) avoids OOD extrapolation that would otherwise inflate the inferred threshold $z^*(x)$. Thus expectile regression is a dataset-grounded surrogate for the implicit action maximization in the epigraph definition, and it is complementary to the decomposition regularizer in (6).

4.2. Practical Loss Functions

Learning proceeds by alternating fitting an action-value model, distilling expectile values, estimating the separate reward and safety envelopes, and enforcing the decomposition constraint. All expectations are empirical averages over minibatches drawn from \mathcal{D} together with z values sampled from a dataset-supported interval $[z_{\min}, z_{\max}]$. The auxiliary Q-target follows from (5),

$$y_Q(x, z, a, x', z') = \min\{\ell(x), \gamma\hat{V}_\theta(x', z')\}, \quad (7)$$

Algorithm 1 Learning the Auxiliary Epigraph Value Function (Epi-Flow)

Require: Offline dataset $\mathcal{D} = \{(x, a, r, \ell, x')\}$, discount factor γ , expectile parameter τ , regularization weight λ_2

- 1: Initialize networks $\hat{Q}_\theta, \hat{V}_\theta, Q_r, V_r, Q_s, V_s$
- 2: **while** not converged **do**
- 3: Sample minibatch $(x, a, r, \ell, x') \sim \mathcal{D}$
- 4: Sample $z \sim [z_{\min}, z_{\max}]$ and compute $z' = (z - r(x))/\gamma$
- 5: **Auxiliary Q-update:**
- 6: $y_Q \leftarrow \min\{\ell(x), \gamma\hat{V}_\theta(x', z')\}$
- 7: Update \hat{Q}_θ by minimizing $\mathcal{L}_{\hat{Q}}$
- 8: **Reward value updates:**
- 9: Update Q_r, V_r using $\mathcal{L}_{Q_r}, \mathcal{L}_{V_r}$
- 10: **Safety value updates:**
- 11: Update Q_s, V_s using $\mathcal{L}_{Q_s}, \mathcal{L}_{V_s}$
- 12: **Expectile value distillation & regularization:**
- 13: Update \hat{V}_θ using $\mathcal{L}_{\hat{V}} + \lambda \cdot \mathcal{L}_{reg}$
- 14: **end while**
- 15: **return** Learned auxiliary value function \hat{V}_θ

and the corresponding squared loss is

$$\mathcal{L}_{\hat{Q}}(\theta) = \mathbb{E}[(y_Q(x, z, a, x', z') - \hat{Q}_\theta(x, z, a))^2], \quad (8)$$

Expectile distillation to the state-value is performed by

$$\mathcal{L}_{\hat{V}}(\theta) = \mathbb{E}[\mathcal{L}^\tau(\hat{Q}_\psi(x, z, a) - \hat{V}_\theta(x, z))], \quad (9)$$

with τ chosen to bias toward the upper data-supported envelope. The reward and safety envelopes are estimated via analogous Q/V losses:

$$\mathcal{L}_{Q_r}(\phi) = \mathbb{E}[(r(x) + \gamma V_r^\phi(x') - Q_r^\phi(x, a))^2], \quad (10)$$

$$\mathcal{L}_{V_r}(\phi) = \mathbb{E}[\mathcal{L}^\tau(Q_r^\phi(x, a) - V_r^\phi(x))], \quad (11)$$

$$\mathcal{L}_{Q_s}(\psi) = \mathbb{E}[(\min\{\ell(x), \gamma V_s^\psi(x')\} - Q_s^\psi(x, a))^2], \quad (12)$$

$$\mathcal{L}_{V_s}(\psi) = \mathbb{E}[\mathcal{L}^\tau(Q_s^\psi(x, a) - V_s^\psi(x))]. \quad (13)$$

The decomposition regularizer is implemented as the one-sided penalty

$$\mathcal{L}_{reg}(\theta) = \mathbb{E} \left[\max \left(0, \hat{V}_\theta(x, z) - \min \{V_r^\phi(x) - z, V_s^\psi(x)\} \right) \right], \quad (14)$$

reduction of this loss would ensure satisfaction of Eq. (6) and the full objective combines the terms:

$$\mathcal{L} = \mathcal{L}_{\hat{V}}(\theta) + \lambda \cdot \mathcal{L}_{reg}(\theta) \quad (15)$$

where the λ control the trade-offs between regression, expectile distillation, envelope fitting, and the decomposition regularizer.

The outcome of this learning procedure is a dataset-consistent auxiliary value function $\hat{V}_\theta(x, z)$ together with reward and safety envelopes $V_r(x)$ and $V_s(x)$. In the next section, we show how these functions will be leveraged to synthesize executable policies in continuous action spaces. The complete learning procedure is summarized in Algorithm 1, and its interaction between the different components is illustrated in Fig. 1.

5. Policy Synthesis via Epigraph-Guided Flow Matching

Given the learned auxiliary value function $\hat{V}_\theta(x, z)$, we now describe how to synthesize a policy that improves performance while respecting the feasibility constraints encoded by the epigraph formulation. For each state x , feasibility induces a maximal admissible performance threshold

$$z^*(x) = \sup\{z \in \mathbb{R} \mid \hat{V}_\theta(x, z) \geq 0\}, \quad (16)$$

which is obtained via binary search over z . Although strict monotonicity is not enforced architecturally, we find that the learned $\hat{V}_\theta(x, z)$ exhibits sufficient empirical monotonicity for stable bisection when combined with interval clamping.

Policy improvement is formulated as a state-wise optimization that favors actions yielding high feasible performance while remaining close to the behavior distribution underlying the offline dataset. Let $\pi_\beta(a \mid x)$ denote the behavior policy. We consider the regularized objective:

$$\pi^*(\cdot \mid x) = \arg \max_{\pi(\cdot \mid x)} \left\{ \mathbb{E}_{a \sim \pi(\cdot \mid x)} [\hat{A}(x, a; z^*(x))] - \frac{1}{\alpha} \text{KL}(\pi(\cdot \mid x) \parallel \pi_\beta(\cdot \mid x)) \right\}. \quad (17)$$

where $\alpha > 0$ is a temperature parameter and $\hat{A}(x, a; z) = \hat{Q}_\theta(x, z, a) - \hat{V}_\theta(x, z)$ denotes the auxiliary advantage evaluated at optimal $z^*(x)$. This objective leads to the following characterization.

Theorem 5.1 (Epigraph-Guided Optimal Policy). *For any state x such that $\pi_\beta(a \mid x) > 0$ on the action support, the solution of (17) is given by the exponential tilting*

$$\pi^*(a \mid x) \propto \pi_\beta(a \mid x) \exp(\alpha \hat{A}(x, a; z^*(x))) \quad (18)$$

For the proof of the theorem 5.1, please refer Appendix A.4. The policy in (18) concentrates probability mass on actions that maximize epigraph-consistent advantage while suppressing actions unsupported by the dataset through the KL regularization. The temperature α controls the trade-off between improvement and adherence to the offline distribution.

To realize the policy in (18) in continuous action spaces, we parameterize π^* implicitly using a conditional flow model

trained via Flow Matching. Let $p_\beta(a \mid x)$ denote the empirical action density induced by the dataset. The target policy corresponds to the reweighted density $p_\beta(a \mid x)w(x, a)$, where

$$w(x, a) = \exp(\alpha \hat{A}(x, a; z^*(x))). \quad (19)$$

Flow Matching learns a time-dependent vector field $v_\zeta(a, x, t)$ whose induced ODE transports samples from a simple base distribution to this weighted target density.

The flow model is trained by minimizing the weighted Flow Matching objective

$$\mathcal{L}_{\text{FM}}(\zeta) = \mathbb{E}_{(x, a) \sim \mathcal{D}, t, \epsilon} \left[w(x, a) \|v_\zeta(a_t, x, t) - u_t(a_t \mid a)\|_2^2 \right], \quad (20)$$

where a_t lies along a predefined probability path from noise to the data action a , and $u_t(a_t \mid a)$ denotes the corresponding target vector field. This construction yields the following recovery result.

Theorem 5.2 (Weighted Flow Matching Policy Recovery). *Let $p_0(a)$ denote a base distribution and let $v_\zeta(a, x, t)$ define a time-dependent vector field inducing the ODE*

$$\frac{da_t}{dt} = v_\zeta(a_t, x, t), \quad a_0 \sim p_0. \quad (21)$$

Let $p_t^\zeta(a \mid x)$ denote the conditional density induced by this flow at time t . Assume sufficient model capacity and exact minimization of the weighted Flow Matching objective (20). Then the terminal density $p_1^\zeta(a \mid x)$ satisfies

$$p_1^\zeta(a \mid x) \propto p_\beta(a \mid x) \exp(\alpha \hat{A}(x, a; z^*(x))), \quad (22)$$

which coincides with the epigraph-guided optimal policy $\pi^(a \mid x)$ defined in (18).*

For the proof of the theorem 5.2, please refer Appendix A.5. At inference time, actions are generated by integrating the learned ODE conditioned on $(x, z^*(x))$. The complete procedure for computing $z^*(x)$, constructing epigraph-guided weights, and training the flow-based policy is summarized in Algorithm 2 and illustrated in Fig. 1.

6. Experiments

To evaluate Epi-Flow, we want to address two core questions: (i) how its safety rate compares to state-of-the-art constrained offline RL baselines; and (ii) how compliance with safety constraints impacts task performance, measured by the cumulative reward $R(x) = \sum_{k=0}^{\infty} \gamma^k \cdot r(x_k)$. By answering these questions we demonstrate that Epi-Flow enables co-optimization of safety and performance, achieving substantially higher safety rates while maintaining competitive cumulative reward.

Baselines: We compare Epi-Flow against a diverse set of safety constrained offline reinforcement learning meth-

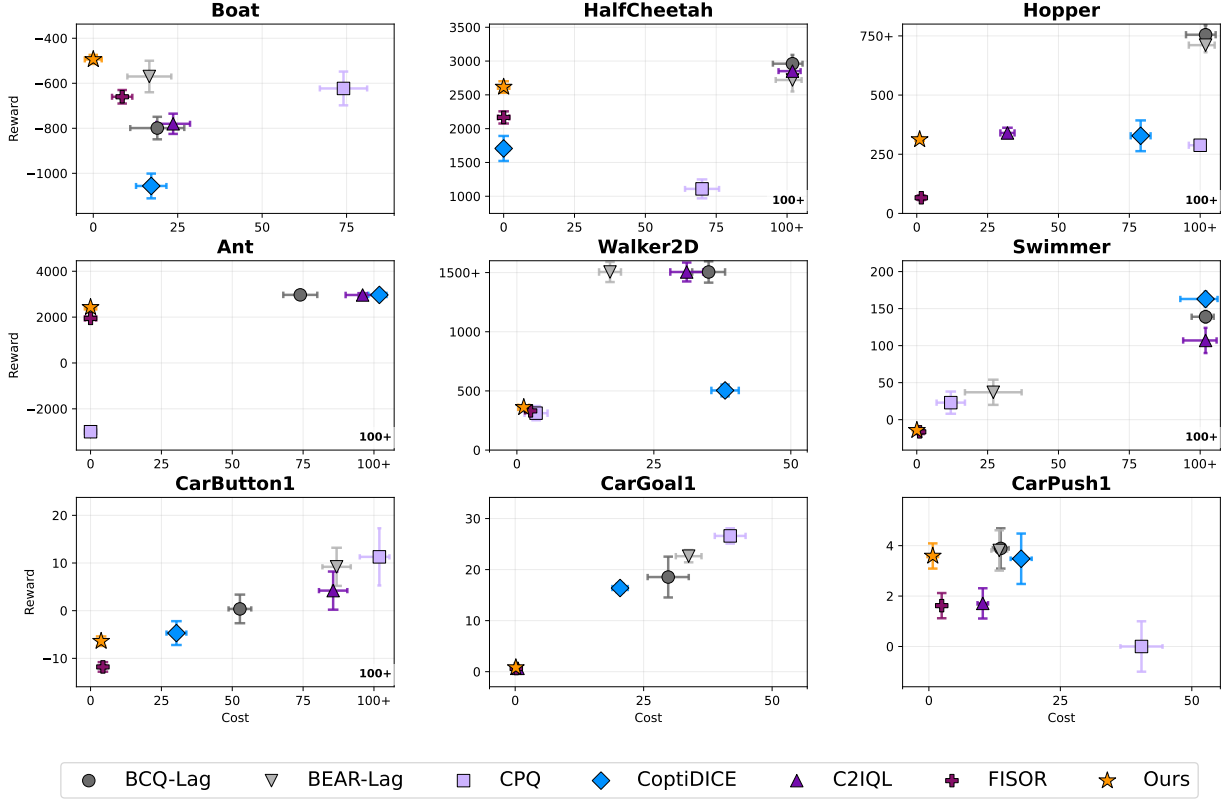


Figure 2. **Evaluation Results:** Results plot for all the environments. Points towards **left** (\leftarrow) are more safe than those on **right** (\rightarrow). Whereas those towards **top** (\uparrow) have higher rewards than those towards **bottom** (\downarrow). Evaluated over 500 episodes and 5 seed values.

ods. For such approaches, we include **BEAR-Lag** (Lagrangian dual version of (Kumar et al., 2019)), **BCQ-Lag** (Lagrangian dual version of (Fujimoto et al., 2019)), **COptiDICE** (Lee et al., 2022), **CPQ** (Xu et al., 2022), **C2IQL** (Liu et al., 2025) and **FISOR** (Zheng et al., 2024). In contrast to these methods, Epi-Flow learns an *auxiliary value function* based policy from offline demonstrations that accounts for future unsafe interactions in advance and therefore, accordingly taking actions that maximize the cumulative reward.

Evaluation Metrics: We evaluate all methods based on (i) *safety/cost*, measured as the total number of safety violations incurred before episode termination, and (ii) *performance*, measured via the cumulative episode rewards. These metrics allow us to assess the trade-off between strict safety enforcement and task performance across different offline RL approaches.

6.1. Experimental Case Studies

For experiments, we test and evaluate our framework against the baselines on a varied range of environments. Below we list all these environments that we use:

- **Safe Boat Navigation:** In our first experiment, we examine a 2-dimensional collision avoidance problem

involving a boat governed by Point mass dynamics in a river with drift velocity that varies with the y-coordinate of the boat. The objective is to ensure safety by avoiding the static obstacles while navigating through the river with varying drift. To evaluate our method against baselines, we randomly sampled 500 initial states. Further details on the system dynamics, state space bounds, and experimental setup are provided in Appendix B.1.

• **Safety Gymnasium:** We also evaluate our framework on Safety Gymnasium environments (Ji et al., 2023) which include Safe Velocity and Safe Navigation Gymnasium environments. Specifically, we evaluate Epi-Flow on high-dimensional MuJoCo tasks like Hopper, Half Cheetah, Swimmer, Walker2D and Ant for Safe Velocity task, and Car Navigation task with 3 navigation environment types: Goal, Push, Button. For the safe velocity task, the objective in each environment is to maximize reward while keeping the agent velocity below the velocity thresholds. For Safe Car Navigation, the objective in each environment type is to avoid the obstacles while maximizing the reward. For evaluation of our method against baselines, we have randomly sampled 500 initial states for each environment.

For all the standard Safety Gymnasium, we retain the

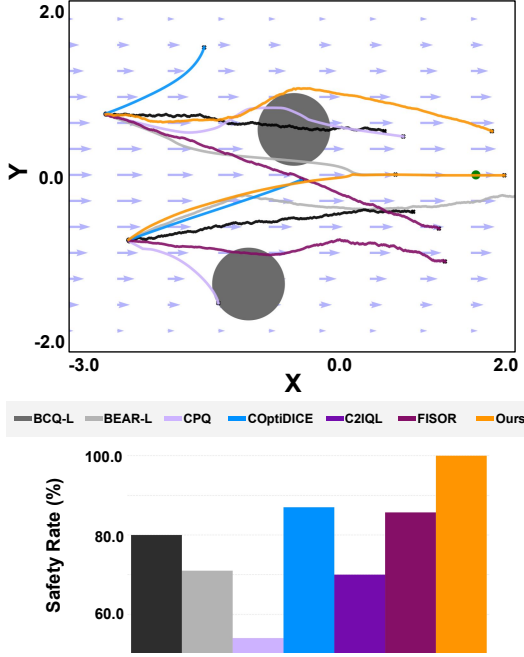


Figure 3. Boat Environment Analysis. (Top): Trajectories for all methods (baselines and ours) rollout from 2 distinct initial states are shown, where the 2 circles are the obstacles with which the agent has to avoid any collision while trying to reach the goal.

original reward and safety-violation metrics from Safety-Gymnasium (Ji et al., 2023) and use the standard DSRL dataset for safe offline RL (Liu et al., 2024b). To evaluate our method against baselines for results, we fixed 500 randomly sampled safe initial states for each environment.

6.2. Results

We evaluate Epi-Flow against a comprehensive set of offline RL baselines across all environments described above. Figure 2 summarizes the results, illustrating how different methods navigate the trade-off between cumulative reward and safety constraint satisfaction. Existing safe offline RL approaches vary widely in their ability to balance these objectives. Lagrangian-based methods such as BEAR-Lag and BCQ-Lag frequently favor reward maximization, resulting in elevated safety violations due to weak constraint enforcement. Other approaches, including COptiDICE, CPQ, and C2IQL, exhibit inconsistent behavior across tasks, alternating between overly conservative policies that sacrifice performance and policies that fail to maintain reliable safety rates. FISOR achieves strong safety performance across environments, but typically does so by adopting conservative policies that limit achievable reward.

In contrast, Epi-Flow consistently attains high safety rates while maintaining strong performance across all evaluated domains, ranging from low-dimensional Boat Navigation to high-dimensional MuJoCo Safe Velocity and Safe Car Navigation tasks. Unlike prior methods that trade reward

for safety or vice versa, Epi-Flow reliably operates in the desirable regime where both objectives are jointly optimized. By leveraging the epigraph-guided auxiliary value function, our approach anticipates future safety violations and allocates performance budgets accordingly, avoiding both excessive conservatism and unsafe reward-seeking. These results demonstrate that Epi-Flow offers a more stable and effective solution for safety-critical offline reinforcement learning than existing constraint-based or filtering-based baselines.

6.3. Ablation Studies

To better understand the design choices and robustness of Epi-Flow, we conduct a series of ablation studies that isolate the effect of key modeling and inference components. Specifically, we examine: (i) the robustness of the learned policy to action perturbations, which probes the stability of epigraph-guided synthesis under execution noise; (ii) sensitivity to the expectile parameter τ , which governs how aggressively the auxiliary value function prioritizes high, dataset-supported feasibility levels; (iii) the effect of the number of action samples used at inference time, highlighting the trade-offs between computation cost, performance, and safety; and (iv) the role of the decomposition regularizer and its weight λ in shaping the learned auxiliary value function and downstream policy behavior. Together, these ablations provide insight into the stability, hyperparameter sensitivity, and practical deployment characteristics of Epi-Flow. Detailed quantitative results and visualizations are reported in Appendix C.

7. Conclusion and Future Work

In this work, we proposed an offline reinforcement learning framework that co-optimizes safety and performance by leveraging an epigraph-based reformulation to convert hard state constraints into a tractable value-based synthesis problem. The method learns an auxiliary feasibility-aware value function via expectile regression and synthesizes executable policies in continuous action spaces using epigraph-guided weighted Flow Matching, while remaining within the support of the offline data and avoiding online exploration. Empirically, the approach achieves consistently low observed safety violations across a range of high-dimensional control tasks while maintaining competitive performance. While several environments exhibit rare or no violations, others show small but non-zero costs, indicating that the learned value functions act as empirical, in-distribution safety certificates rather than formal worst-case guarantees. Future work includes integrating formal verification methods, such as conformal prediction or Lipschitz-based certification, and extending the framework to stochastic and adversarial settings using uncertainty-aware and robust optimization techniques to handle distributional shift and disturbances.

Impact Statement

This work introduces a robust methodology for co-optimizing safety and performance in autonomous systems within the offline reinforcement learning paradigm. By utilizing an epigraph-based reformulation to transform hard state constraints into a tractable optimization problem, our framework enables the extraction of reliable policies from pre-collected, static datasets without the risks associated with online exploration. The integration of weighted Flow Matching ensures that the synthesized controllers remain strictly faithful to the safe regions of the data distribution, effectively mitigating the dangers of over-estimation in safety-critical environments. These advancements provide a scalable path for deploying reliable agents in high-dimensional domains, such as robotics and autonomous mobility, where learning exclusively from demonstrations is a prerequisite for operational trust and public safety.

References

Achiam, J., Held, D., Tamar, A., and Abbeel, P. Constrained policy optimization. In *Proceedings of the 34th International Conference on Machine Learning - Volume 70, ICML'17*, pp. 22–31. JMLR.org, 2017.

Albergo, M. S. and Vanden-Eijnden, E. Building normalizing flows with stochastic interpolants. In *The Eleventh International Conference on Learning Representations, 2023*. URL <https://openreview.net/forum?id=li7qeBbCR1t>.

Alles, M., Chen, N., van der Smagt, P., and Cseke, B. Flowq: Energy-guided flow policies for offline reinforcement learning, 2025. URL <https://arxiv.org/abs/2505.14139>.

Alshiekh, M., Bloem, R., Ehlers, R., Könighofer, B., Niekum, S., and Topcu, U. Safe reinforcement learning via shielding. *Proceedings of the AAAI Conference on Artificial Intelligence*, 32(1), Apr. 2018. doi: 10.1609/aaai.v32i1.11797. URL <https://ojs.aaai.org/index.php/AAAI/article/view/11797>.

Altarovici, A., Bokanowski, O., and Zidani, H. A general hamilton-jacobi framework for non-linear state-constrained control problems. *ESAIM: Control, Optimisation and Calculus of Variations*, 19(2):337–357, 2013.

Altman, E. *Constrained Markov decision processes*. Routledge, 2021.

Baird, L. Residual algorithms: Reinforcement learning with function approximation. In *Machine Learning Proceedings 1995*, pp. 30–37. Elsevier, 1995.

Boyd, S. and Vandenberghe, L. *Convex optimization*. Cambridge university press, 2004.

Chen, H., Lu, C., Ying, C., Su, H., and Zhu, J. Offline reinforcement learning via high-fidelity generative behavior modeling. In *The Eleventh International Conference on Learning Representations, 2023*. URL <https://openreview.net/forum?id=42zs3qa2kpy>.

Chen, L., Lu, K., Rajeswaran, A., Lee, K., Grover, A., Laskin, M., Abbeel, P., Srinivas, A., and Mordatch, I. Decision transformer: Reinforcement learning via sequence modeling. *Advances in neural information processing systems*, 34:15084–15097, 2021.

Chow, Y., Ghavamzadeh, M., Janson, L., and Pavone, M. Risk-constrained reinforcement learning with percentile risk criteria. *The Journal of Machine Learning Research*, 18(1):6070–6120, 2017a.

Chow, Y. T., Darbon, J., Osher, S., and Yin, W. Algorithm for overcoming the curse of dimensionality for time-dependent non-convex hamilton–jacobi equations arising from optimal control and differential games problems. *Journal of Scientific Computing*, 73:617–643, 2017b.

Fisac, J. F., Lugovoy, N. F., Rubies-Royo, V., Ghosh, S., and Tomlin, C. J. Bridging hamilton–jacobi safety analysis and reinforcement learning. In *2019 International Conference on Robotics and Automation (ICRA)*, pp. 8550–8556, 2019. doi: 10.1109/ICRA.2019.8794107.

Fujimoto, S., Hoof, H., and Meger, D. Addressing function approximation error in actor-critic methods. In *International conference on machine learning*, pp. 1587–1596. PMLR, 2018.

Fujimoto, S., Meger, D., and Precup, D. Off-policy deep reinforcement learning without exploration. In *International conference on machine learning*, pp. 2052–2062. PMLR, 2019.

Gottesman, O., Johansson, F., Komorowski, M., Faisal, A., Sontag, D., Doshi-Velez, F., and Celi, L. A. Guidelines for reinforcement learning in healthcare. *Nature medicine*, 25(1):16–18, 2019.

Hansen-Estruch, P., Kostrikov, I., Janner, M., Kuba, J. G., and Levine, S. Idql: Implicit q-learning as an actor-critic method with diffusion policies, 2023. URL <https://arxiv.org/abs/2304.10573>.

Janner, M., Du, Y., Tenenbaum, J., and Levine, S. Planning with diffusion for flexible behavior synthesis. In *International Conference on Machine Learning*, pp. 9902–9915. PMLR, 2022.

Ji, J., Zhang, B., Zhou, J., Pan, X., Huang, W., Sun, R., Geng, Y., Zhong, Y., Dai, J., and Yang, Y. Safety gymnasium: A unified safe reinforcement learning benchmark. In *Thirty-seventh Conference on Neural Information Processing Systems Datasets and Benchmarks Track*,

2023. URL <https://openreview.net/forum?id=WZmlxIuIGR>.

Kiran, B. R., Sobh, I., Talpaert, V., Mannion, P., Al Salab, A. A., Yogamani, S., and Pérez, P. Deep reinforcement learning for autonomous driving: A survey. *IEEE transactions on intelligent transportation systems*, 23(6):4909–4926, 2021.

Kostrikov, I., Nair, A., and Levine, S. Offline reinforcement learning with implicit q-learning. In *International Conference on Learning Representations*, 2022.

Kumar, A., Fu, J., Soh, M., Tucker, G., and Levine, S. Stabilizing off-policy q-learning via bootstrapping error reduction. *Advances in neural information processing systems*, 32, 2019.

Kumar, A., Zhou, A., Tucker, G., and Levine, S. Conservative q-learning for offline reinforcement learning. In Larochelle, H., Ranzato, M., Hadsell, R., Balcan, M., and Lin, H. (eds.), *Advances in Neural Information Processing Systems*, volume 33, pp. 1179–1191. Curran Associates, Inc., 2020. URL https://proceedings.neurips.cc/paper_files/paper/2020/file/0d2b2061826a5df3221116a5085a6052-Paper.pdf.

Lee, J., Jeon, W., Lee, B., Pineau, J., and Kim, K.-E. Optidice: Offline policy optimization via stationary distribution correction estimation. In *International Conference on Machine Learning*, pp. 6120–6130. PMLR, 2021.

Lee, J., Paduraru, C., Mankowitz, D. J., Heess, N., Precup, D., Kim, K.-E., and Guez, A. COptiDICE: Offline constrained reinforcement learning via stationary distribution correction estimation. In *International Conference on Learning Representations*, 2022. URL <https://openreview.net/forum?id=FLA55mBee6Q>.

Levine, S., Kumar, A., Tucker, G., and Fu, J. Offline reinforcement learning: Tutorial, review, and perspectives on open problems, 2020. URL <https://arxiv.org/abs/2005.01643>.

Li, J., Zhan, X., Xu, H., Zhu, X., Liu, J., and Zhang, Y.-Q. When data geometry meets deep function: Generalizing offline reinforcement learning. In *The Eleventh International Conference on Learning Representations*, 2023.

Lin, Q., Tang, B., Wu, Z., Yu, C., Mao, S., Xie, Q., Wang, X., and Wang, D. Safe offline reinforcement learning with real-time budget constraints. In *International Conference on Machine Learning*, 2023.

Lipman, Y., Chen, R. T. Q., Ben-Hamu, H., Nickel, M., and Le, M. Flow matching for generative modeling. In *The Eleventh International Conference on Learning Representations*, 2023. URL <https://openreview.net/forum?id=PqvMRDCJT9t>.

Liu, X., Zhang, X., Ma, J., Peng, J., and qiang liu. Instaflow: One step is enough for high-quality diffusion-based text-to-image generation. In *The Twelfth International Conference on Learning Representations*, 2024a. URL <https://openreview.net/forum?id=1k4yZbbDqX>.

Liu, Z., Guo, Z., Yao, Y., Cen, Z., Yu, W., Zhang, T., and Zhao, D. Constrained decision transformer for offline safe reinforcement learning. In *International Conference on Machine Learning*, 2023.

Liu, Z., Guo, Z., Lin, H., Yao, Y., Zhu, J., Cen, Z., Hu, H., Yu, W., Zhang, T., Tan, J., and Zhao, D. Datasets and benchmarks for offline safe reinforcement learning. *Journal of Data-centric Machine Learning Research*, 2024b.

Liu, Z., Li, X., and Zhang, J. C2IQL: Constraint-conditioned implicit q-learning for safe offline reinforcement learning. In *Forty-second International Conference on Machine Learning*, 2025. URL <https://openreview.net/forum?id=97N3XNtFwy>.

Mitchell, I. A toolbox of level set methods. <http://www.cs.ubc.ca/mitchell/ToolboxLS/toolboxLS.pdf>, 2004.

Nair, A., Gupta, A., Dalal, M., and Levine, S. Awac: Accelerating online reinforcement learning with offline datasets, 2021. URL <https://arxiv.org/abs/2006.09359>.

Park, S., Li, Q., and Levine, S. Flow q-learning. In *International Conference on Machine Learning (ICML)*, 2025.

Peng, X. B., Kumar, A., Zhang, G., and Levine, S. Advantage-weighted regression: Simple and scalable off-policy reinforcement learning, 2019. URL <https://arxiv.org/abs/1910.00177>.

So, O., Ge, C., and Fan, C. Solving minimum-cost reach avoid using reinforcement learning. In *The Thirty-eighth Annual Conference on Neural Information Processing Systems*, 2024. URL <https://openreview.net/forum?id=jzngdJQ21Y>.

Soner, H. M. Optimal control with state-space constraint i. *SIAM Journal on Control and Optimization*, 24(3):552–561, 1986. doi: 10.1137/0324032. URL <https://doi.org/10.1137/0324032>.

Stooke, A., Achiam, J., and Abbeel, P. Responsive safety in reinforcement learning by PID lagrangian

methods. In III, H. D. and Singh, A. (eds.), *Proceedings of the 37th International Conference on Machine Learning*, volume 119 of *Proceedings of Machine Learning Research*, pp. 9133–9143. PMLR, 13–18 Jul 2020. URL <https://proceedings.mlr.press/v119/stooke20a.html>.

Sutton, R. S., Barto, A. G., et al. Reinforcement learning. *Journal of Cognitive Neuroscience*, 11(1):126–134, 1999.

Tayal, M., Zhang, H., Jagtap, P., Clark, A., and Kolathaya, S. Learning a formally verified control barrier function in stochastic environment. In *2024 IEEE 63rd Conference on Decision and Control (CDC)*, pp. 4098–4104, 2024. doi: 10.1109/CDC56724.2024.10886052.

Tayal, M., Singh, A., Kolathaya, S., and Bansal, S. A physics-informed machine learning framework for safe and optimal control of autonomous systems. In *Forty-second International Conference on Machine Learning*, 2025a. URL <https://openreview.net/forum?id=SrfwiloGQF>.

Tayal, M., Tayal, M., Singh, A., Kolathaya, S., and Prakash, R. V-ocbf: Learning safety filters from offline data via value-guided offline control barrier functions. *arXiv preprint arXiv:2512.10822*, 2025b.

Tessler, C., Mankowitz, D. J., and Mannor, S. Reward constrained policy optimization. In *International Conference on Learning Representations*, 2018.

Wang, H., Dhande, A., and Bansal, S. Cooptimizing safety and performance with a control-constrained formulation. *IEEE Control Systems Letters*, 8:2739–2744, 2024. doi: 10.1109/LCSYS.2024.3511429.

Xu, H., Zhan, X., and Zhu, X. Constraints penalized q-learning for safe offline reinforcement learning. In *Proceedings of the AAAI Conference on Artificial Intelligence*, volume 36, pp. 8753–8760, 2022.

Zhang, S., Zhang, W., and Gu, Q. Energy-weighted flow matching for offline reinforcement learning. In *The Thirteenth International Conference on Learning Representations*, 2025. URL <https://openreview.net/forum?id=HA0oLUVuGI>.

Zhao, W., He, T., Chen, R., Wei, T., and Liu, C. Safe reinforcement learning: A survey. *arXiv preprint arXiv:2302.03122*, 2023.

Zheng, Y., Li, J., Yu, D., Yang, Y., Li, S. E., Zhan, X., and Liu, J. Safe offline reinforcement learning with feasibility-guided diffusion model. In *International Conference on Learning Representations*, 2024. URL <https://openreview.net/forum?id=cM95sT3gM3>.

A. Theoretical Insights

A.1. Derivation of the Epigraph Reformulation

In this section, we formally derive the auxiliary epigraph value function and prove its equivalence to the original state-constrained objective. We show that maximizing the constrained value is equivalent to finding the maximal level-set of an unconstrained auxiliary value function defined over an augmented state space.

A.1.1. PROBLEM FORMULATION

Consider a deterministic Markov Decision Process (MDP) with state dynamics $x_{k+1} = f(x_k, a_k)$ and a reward function $r(x_k)$. We enforce a hard state constraint $\ell(x_k) \geq 0$ for all time steps $k \geq t$.

Let Π denote the set of all admissible policies. The state-constrained value function $V(x_t)$ is defined as the supremum of the cumulative discounted return subject to safety constraints:

$$V(x_t) := \sup_{\pi \in \Pi} \left\{ \sum_{k=t}^{\infty} \gamma^{k-t} r(x_k) \mid \ell(x_k) \geq 0, \forall k \geq t \right\}. \quad (23)$$

A.1.2. EPIGRAPH VALUE FUNCTION

We introduce an auxiliary scalar decision variable $z_t \in \mathbb{R}$, which represents a candidate performance threshold (Boyd & Vandenberghe, 2004). We define the *auxiliary epigraph value function* $\hat{V}(x_t, z_t)$ as the optimal value of a maximin objective that jointly considers the return margin and the safety margin:

$$\hat{V}(x_t, z_t) := \sup_{\pi \in \Pi} \min \left\{ \sum_{k=t}^{\infty} \gamma^{k-t} r(x_k) - z_t, \inf_{s \geq t} \gamma^{s-t} \ell(x_s) \right\}. \quad (24)$$

Proposition A.1 (Equivalence of Epigraph Formulation). *The original constrained value function $V(x_t)$ can be recovered from the zero-level set of the auxiliary value function $\hat{V}(x_t, z_t)$. Specifically:*

$$V(x_t) = \sup \{z_t \in \mathbb{R} \mid \hat{V}(x_t, z_t) \geq 0\}. \quad (25)$$

Proof. We proceed by transforming the optimization problem in (23) using the epigraph form. Let $J(\pi; x_t) = \sum_{k=t}^{\infty} \gamma^{k-t} r(x_k)$ denote the return and $S(\pi; x_t) = \inf_{s \geq t} \ell(x_s)$ denote the safety margin of a policy. The constraint $\ell(x_k) \geq 0 \forall k$ is equivalent to $S(\pi; x_t) \geq 0$.

The original problem can be rewritten by introducing the variable z_t to represent the objective value:

$$\begin{aligned} V(x_t) &= \sup_{\pi, z_t} z_t \\ \text{s.t. } &J(\pi; x_t) \geq z_t, \\ &S(\pi; x_t) \geq 0. \end{aligned} \quad (26)$$

The two inequality constraints must hold simultaneously. This is logically equivalent to requiring the minimum of the constraint residuals to be non-negative. Note that $J(\pi; x_t) \geq z_t \iff J(\pi; x_t) - z_t \geq 0$. Thus, the constraints are satisfied if and only if:

$$\min \{J(\pi; x_t) - z_t, S(\pi; x_t)\} \geq 0. \quad (27)$$

Substituting this back into the optimization problem:

$$\begin{aligned} V(x_t) &= \sup_{z_t} \{z_t \mid \exists \pi \in \Pi \text{ s.t. } \min \{J(\pi; x_t) - z_t, S(\pi; x_t)\} \geq 0\} \\ &= \sup_{z_t} \left\{ z_t \mid \sup_{\pi \in \Pi} \min \{J(\pi; x_t) - z_t, S(\pi; x_t)\} \geq 0 \right\}. \end{aligned} \quad (28)$$

To align this with the definition in (24), we observe that the sign of the safety term is invariant under multiplication by a positive discount factor $\gamma^{s-t} > 0$. Therefore, $S(\pi; x_t) \geq 0$ is equivalent to $\inf_{s \geq t} \gamma^{s-t} \ell(x_s) \geq 0$.

Replacing the safety term, the inner optimization becomes exactly $\hat{V}(x_t, z_t)$. Thus:

$$V(x_t) = \sup\{z_t \in \mathbb{R} \mid \hat{V}(x_t, z_t) \geq 0\}. \quad (29)$$

□

Remark on Discounted Safety. In (24), the safety constraint $\ell(x_s)$ is scaled by the discount factor γ^{s-t} . Since $\gamma \in (0, 1)$, this scaling does not alter the sign of the term, nor does it change the feasibility boundary (i.e., $\gamma^{s-t}\ell(x_s) \geq 0 \iff \ell(x_s) \geq 0$). This modification is introduced solely to ensure the resulting operator is a contraction, enabling the use of standard discrete-time Bellman recursions for learning \hat{V} .

A.2. Theorem (4.1)

Theorem 4.1 (Epigraph Value Recursion) Consider a deterministic SC-MDP with bounded reward and discount factor $\gamma \in (0, 1)$. Given a transition $(x_t, a_t, r_t, \ell_t, x_{t+1})$ and the epigraph update $z_{t+1} = (z_t - r(x_t))/\gamma$, the epigraph value function $\hat{V}(x_t, z_t)$ satisfies the recursion

$$\hat{V}(x_t, z_t) = \min \{\ell(x_t), \gamma \hat{V}(x_{t+1}, z_{t+1})\}.$$

Proof. We begin from the definition of the auxiliary value function in (3). For any policy π and initial state x_t , decompose the two terms inside the minimum.

First, the discounted return term admits the decomposition

$$\sum_{k=t}^{\infty} \gamma^{k-t} r(x_k) - z_t = \gamma \left(\sum_{k=t+1}^{\infty} \gamma^{k-(t+1)} r(x_k) - z_{t+1} \right), \quad (30)$$

where the relation follows from the definition $z_{t+1} = (z_t - r(x_t))/\gamma$.

Second, the discounted safety term satisfies

$$\min_{s \geq t} \gamma^{s-t} \ell(x_s) = \min \{\ell(x_t), \gamma \min_{s \geq t+1} \gamma^{s-(t+1)} \ell(x_s)\}. \quad (31)$$

Substituting these decompositions into (3) yields

$$\hat{V}(x_t, z_t) = \sup_{\pi} \min \left\{ \gamma \left(\sum_{k=t+1}^{\infty} \gamma^{k-(t+1)} r(x_k) - z_{t+1} \right), \ell(x_t), \gamma \min_{s \geq t+1} \gamma^{s-(t+1)} \ell(x_s) \right\}. \quad (32)$$

Since $\ell(x_t)$ is independent of future actions, and $\gamma > 0$, the minimum can be reordered as

$$\hat{V}(x_t, z_t) = \min \left\{ \ell(x_t), \gamma \sup_{\pi} \min \left(\sum_{k=t+1}^{\infty} \gamma^{k-(t+1)} r(x_k) - z_{t+1}, \min_{s \geq t+1} \gamma^{s-(t+1)} \ell(x_s) \right) \right\}. \quad (33)$$

Recognizing the inner supremum as the definition of $\hat{V}(x_{t+1}, z_{t+1})$ completes the proof and yields the recursion (5). □

A.3. Effect of the Decomposition Regularizer on Epigraph Sensitivity

This appendix analyzes the effect of the decomposition-based regularizer (Eq. (14)) on the learned auxiliary epigraph value function $\hat{V}(x, z)$. Figure 4 shows contour plots of \hat{V} evaluated at multiple values of z , comparing the unregularized objective with the regularized variant using $\lambda = 0.25$. In the absence of regularization, the learned \hat{V} exhibits nearly identical contour geometry across different z , indicating weak sensitivity to the epigraph variable. This behavior is consistent with the analysis in Section 4, i.e., although z_t appears in the recursion, the Bellman update does not explicitly enforce conditioning on z , allowing the network to collapse to a representation that largely ignores the epigraph dimension.

Introducing the decomposition regularizer restores meaningful dependence on z . The regularizer enforces the inequality $\hat{V}(x, z) \leq \min\{V_r(x) - z, V_s(x)\}$, which injects an explicit linear dependence on z through the $V_r(x) - z$ term. As a result, the learned \hat{V} must adapt as z varies in order to remain feasible, leading to visibly distinct level sets across different z values in the regularized case. This effect prevents uncontrolled drift along the epigraph dimension and ensures that \hat{V} encodes a nontrivial performance envelope.

Crucially, restoring sensitivity to z is necessary for reliable extraction of the state-wise threshold $z^*(x) = \sup\{z \mid \hat{V}(x, z) \geq 0\}$. When \hat{V} is nearly invariant to z , this threshold becomes ill-defined and unstable, undermining policy synthesis. The regularizer therefore plays a structural role as it does not impose additional conservatism, but instead ensures that the learned auxiliary value function preserves the intended semantics of the epigraph formulation. Additionally, an ablation study on different values of λ is provided in Section C.4.

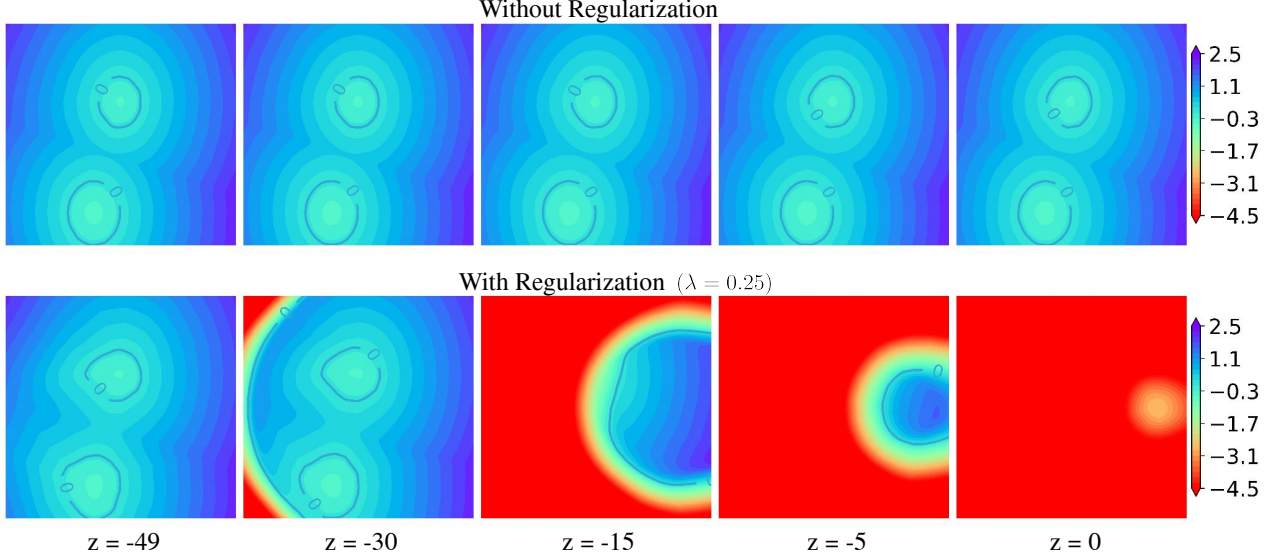


Figure 4. Auxiliary epigraph value function $\hat{V}_\theta(x, z)$. (Top) Learned without the decomposition regularizer, where \hat{V}_θ exhibits weak sensitivity to the epigraph variable z and similar contour structure across different z values. (Bottom) Learned with the regularizer ($\lambda = 0.25$), which restores meaningful dependence on z and yields distinct level sets consistent with the epigraph formulation.

Remark: We would like to emphasize that the decomposition regularizer loss \mathcal{L}_{reg} and the Bellman recursive loss $\mathcal{L}_{\hat{V}}$ play distinct, non-redundant roles. The regularizer acts as a one-sided penalty that defines the valid search space. In the absence of the recursive loss $\mathcal{L}_{\hat{V}}$, the optimization would degenerate to a trivial solution where $\hat{V}(x, z) \rightarrow -\infty$, satisfying the inequality strictly but vacuously. The Bellman recursion is therefore essential, as it drives the value estimate upward to identify the tightest feasible boundary supported by the dataset dynamics.

A.4. Theorem (5.1)

Theorem 5.1 (Epigraph-Guided Optimal Policy) For any state x such that $\pi_\beta(a \mid x) > 0$ on the action support, the solution of (17) is given by the exponential tilting

$$\pi^*(a \mid x) \propto \pi_\beta(a \mid x) \exp(\alpha \hat{A}(x, a; z^*(x)))$$

Proof. To find the optimal policy $\pi^*(\cdot \mid x)$ that maximizes the objective in (17), we consider the Lagrangian \mathcal{L} with the multiplier λ for the normalization constraint $\int \pi(a \mid x) da = 1$:

$$\mathcal{L}(\pi, \lambda) = \int \pi(a \mid x) \hat{A}(x, a; z^*(x)) da - \frac{1}{\alpha} \int \pi(a \mid x) \log \frac{\pi(a \mid x)}{\pi_\beta(a \mid x)} da + \lambda \left(1 - \int \pi(a \mid x) da \right).$$

Taking the functional derivative with respect to $\pi(a|x)$ and setting it to zero gives:

$$\frac{\partial \mathcal{L}}{\partial \pi(a|x)} = \hat{A}(x, a; z^*(x)) - \frac{1}{\alpha} \left(\log \frac{\pi(a|x)}{\pi_\beta(a|x)} + 1 \right) - \lambda = 0.$$

Rearranging the terms to isolate the log-ratio, we obtain:

$$\log \frac{\pi(a|x)}{\pi_\beta(a|x)} = \alpha \hat{A}(x, a; z^*(x)) - (\alpha \lambda + 1).$$

Applying the exponential function to both sides results in:

$$\pi(a|x) = \pi_\beta(a|x) \exp \left(\alpha \hat{A}(x, a; z^*(x)) \right) \exp(-\alpha \lambda - 1).$$

Since $\exp(-\alpha \lambda - 1)$ is constant with respect to the action a , it serves as the partition function $1/Z(x)$ to ensure the distribution integrates to one. Thus, we arrive at the proportional form:

$$\pi^*(a|x) \propto \pi_\beta(a|x) \exp \left(\alpha \hat{A}(x, a; z^*(x)) \right).$$

□

A.5. Theorem (5.2)

Before presenting the proof for theorem 5.2, we first establish known concepts for Flow Matching that will be used to prove the theorem.

Preliminaries on Flow Matching. Flow Matching (Lipman et al., 2023; Liu et al., 2024a; Albergo & Vanden-Eijnden, 2023) has emerged as a robust framework for training Continuous Normalizing Flows (CNFs) without the need for expensive simulation during training. While diffusion-based models have shown great success, Flow Matching often demonstrates superior empirical performance and improved sampling efficiency by learning straighter trajectories in the probability space.

Let $q_1(\mathbf{x}_1)$ be the unknown data distribution from which we have a dataset $\mathcal{D} = \{\mathbf{x}_1^i\}_{i=1}^D$. The goal of Flow Matching is to construct a time-dependent vector field $\mathbf{v}_\theta(\mathbf{x}_t, t) : \mathbb{R}^d \times [0, 1] \rightarrow \mathbb{R}^d$ that defines a probability path p_t between a simple noise prior $p_0(\mathbf{x}_0) = \mathcal{N}(\mathbf{0}, \mathbf{I})$ and the target data distribution q_1 .

The generative process is characterized by an Ordinary Differential Equation (ODE):

$$\frac{d\mathbf{x}_t}{dt} = \mathbf{v}_\theta(\mathbf{x}_t, t), \quad t \in [0, 1]. \quad (34)$$

Starting from $\mathbf{x}_0 \sim p_0$, the solution to this ODE at $t = 1$ yields a sample $\mathbf{x}_1 \sim p_1 \approx q_1$.

To bypass the intractable marginal vector field during training, Flow Matching employs the Conditional Flow Matching (CFM) objective. We define a conditional probability path $p_t(\mathbf{x}_t|\mathbf{x}_1)$ and a corresponding conditional vector field $\mathbf{u}_t(\mathbf{x}_t|\mathbf{x}_1)$. For the case of *Optimal Transport* (OT), which yields straight-line paths, the conditional path and vector field are defined as:

$$\mathbf{x}_t = \psi_t(\mathbf{x}_1) = (1-t)\mathbf{x}_0 + t\mathbf{x}_1, \quad (35)$$

$$\mathbf{u}_t(\mathbf{x}_t|\mathbf{x}_1) = \mathbf{x}_1 - \mathbf{x}_0. \quad (36)$$

The network \mathbf{v}_θ is optimized to match this conditional velocity via the following MSE loss:

$$\mathcal{L}_{\text{CFM}}(\theta) = \mathbb{E}_{t \sim \mathcal{U}([0, 1]), \mathbf{x}_1 \sim q_1, \mathbf{x}_0 \sim p_0} [\|\mathbf{v}_\theta(\mathbf{x}_t, t) - (\mathbf{x}_1 - \mathbf{x}_0)\|_2^2]. \quad (37)$$

Upon convergence, the learned vector field \mathbf{v}_θ approximates the marginal vector field $\mathbb{E}_{q_1} [\mathbf{u}_t(\mathbf{x}_t|\mathbf{x}_1) \frac{p_t(\mathbf{x}_t|\mathbf{x}_1)}{p_t(\mathbf{x}_t)}]$ (Lipman et al., 2023).

Next we will proceed with proving the theorem 5.2.

Theorem 5.2 (Weighted Flow Matching Policy Recovery) Let $p_0(a)$ denote a base distribution and let $v_\zeta(a, x, t)$ define a time-dependent vector field inducing the ODE

$$\frac{da_t}{dt} = v_\zeta(a_t, x, t), \quad a_0 \sim p_0.$$

Let $p_t^\zeta(a | x)$ denote the conditional density induced by this flow at time t . Assume sufficient model capacity and exact minimization of the weighted Flow Matching objective (20). Then the terminal density $p_1^\zeta(a | x)$ satisfies

$$p_1^\zeta(a | x) \propto p_\beta(a | x) \exp(\alpha \hat{A}(x, a; z^*(x))),$$

which coincides with the epigraph-guided optimal policy $\pi^*(a | x)$ defined in (18).

Proof. We demonstrate that the terminal density induced by minimizing the weighted Flow Matching objective recovers the epigraph-guided optimal policy.

Given a dataset \mathcal{D} where actions are distributed according to the behavior policy $\pi_\beta(a | x)$, we define the weighted Flow Matching (WFM) objective as:

$$\mathcal{L}_{\text{FM}}(\zeta) = \mathbb{E}_{x \sim \mathcal{D}, a \sim \pi_\beta(\cdot | x), t \sim \mathcal{U}[0, 1], \epsilon \sim p(\epsilon)} \left[w(x, a) \|v_\zeta(a_t, x, t) - u_t(a_t | a)\|_2^2 \right] \quad (38)$$

where $a_t = \psi_t(a, \epsilon)$ is a point along a predefined probability path from noise to the data action, $u_t(a_t | a) = \frac{d}{dt} \psi_t(a, \epsilon)$ is the target vector field (Lipman et al., 2023), and the epigraph-guided weight is defined as $w(x, a) = \exp(\alpha \hat{A}(x, a; z^*))$ (Theorem 5.1).

For a fixed state x and time t , the objective in (38) is a weighted mean squared error. Assuming sufficient model capacity, the global minimizer v^* is the weighted conditional expectation of the target vector field:

$$v^*(a_t, x, t) = \frac{\mathbb{E}_{a \sim \pi_\beta, \epsilon \sim p(\epsilon)} [w(x, a) \cdot \mathbb{1}(\psi_t(a, \epsilon) = a_t) \cdot u_t(a_t | a)]}{\mathbb{E}_{a \sim \pi_\beta, \epsilon \sim p(\epsilon)} [w(x, a) \cdot \mathbb{1}(\psi_t(a, \epsilon) = a_t)]} \quad (39)$$

Using the properties of the conditional probability path $p_t(a_t | a)$, we express these expectations as integrals over the action space:

$$v^*(a_t, x, t) = \frac{\int \pi_\beta(a | x) w(x, a) p_t(a_t | a) u_t(a_t | a) da}{\int \pi_\beta(a | x) w(x, a) p_t(a_t | a) da} \quad (40)$$

Relation to the Continuity Equation. Let $q_t(a_t | x)$ be the time-dependent marginal density induced by the behavior policy and the epigraph-guided weights:

$$q_t(a_t | x) = \int \pi_\beta(a | x) w(x, a) p_t(a_t | a) da \quad (41)$$

From the principle of Flow Matching (Lipman et al., 2023), a vector field v generates a density path p_t if it satisfies the continuity equation $\frac{\partial p_t}{\partial t} + \nabla \cdot (p_t v) = 0$. The vector field v^* defined in (40) is the unique field that generates the weighted marginal path $q_t(a_t | x)$, normalized by the state-dependent partition function $Z(x) = \int \pi_\beta(a | x) w(x, a) da$. Thus, the flow $\frac{da_t}{dt} = v^*(a_t, x, t)$ induces the density:

$$p_t^\zeta(a_t | x) = \frac{q_t(a_t | x)}{\int q_t(a' | x) da'} = \frac{\int \pi_\beta(a | x) w(x, a) p_t(a_t | a) da}{\int \pi_\beta(a | x) w(x, a) da} \quad (42)$$

Convergence to Terminal Density. The probability path ψ_t is constructed such that at $t = 0$, p_0 is a base distribution, and at $t = 1$, the conditional density $p_1(a_1 | a)$ approaches a Dirac delta distribution $\delta(a_1 - a)$. Taking the limit as $t \rightarrow 1$:

$$p_1^\zeta(a | x) = \lim_{t \rightarrow 1} \frac{\int \pi_\beta(a' | x) w(x, a') p_t(a | a') da'}{\int \pi_\beta(a' | x) w(x, a') da'} \quad (43)$$

Applying the delta property simplifies the numerator:

$$p_1^\zeta(a|x) = \frac{\pi_\beta(a|x)w(x,a)}{\int \pi_\beta(a'|x)w(x,a')da'} \quad (44)$$

Substituting $w(x,a) = \exp(\alpha\hat{A}(x,a;z^*))$ from Section 5:

$$p_1^\zeta(a|x) = \frac{\pi_\beta(a|x) \exp(\alpha\hat{A}(x,a;z^*))}{\int \pi_\beta(a'|x) \exp(\alpha\hat{A}(x,a';z^*))da'} \quad (45)$$

This establishes the proportionality $p_1^\zeta(a|x) \propto \pi_\beta(a|x) \exp(\alpha\hat{A}(x,a;z^*))$. By Theorem 5.1, this terminal density matches the exact form of the epigraph-guided optimal policy $\pi^*(a|x)$. \square

Based on the above theorems and proofs, following is the practical algorithm for learning the Flow Matching based policy in the Algorithm block 2.

Algorithm 2 Epigraph-Guided Flow Matching Policy Extraction

Require: Offline dataset \mathcal{D} , auxiliary value functions \hat{V}_θ and \hat{Q}_θ , temperature α , Gaussian prior p_0 .

Ensure: Learned vector field v_ζ for optimal policy π^* .

- 1: Initialize policy parameters ζ .
- 2: **while** not converged **do**
- 3: Sample transitions $(x, a) \sim \mathcal{D}$.
- 4: Find performance envelope $z^*(x) = \sup\{z \mid \hat{V}_\theta(x, z) \geq 0\}$ via binary search
- 5: Sample time $t \sim \mathcal{U}[0, 1]$ and noise $\epsilon \sim p_0$
- 6: Construct $a_t = (1-t)\epsilon + ta$ and target velocity $u_t = a - \epsilon$
- 7: Compute guidance weight $w = \exp(\alpha\hat{A}(x, a; z^*(x)))$
- 8: Update $\zeta \leftarrow \zeta - \eta \nabla_\zeta w \|v_\zeta(a_t, x, t) - u_t\|^2$
- 9: **end while**

A.6. Expectile Regression

Expectile regression is a classical tool in statistics and econometrics for estimating asymmetric statistics of a random variable. For a random variable X , the τ -expectile is defined as the minimizer of the asymmetric least-squares problem

$$m_\tau = \arg \min_m \mathbb{E}_{x \sim X} [L^\tau(x - m)], \quad (46)$$

where $L_\tau(y) = |\tau - \mathbf{1}(y < 0)|y^2$.

When $\tau > 0.5$, this loss assigns more weight to samples above the estimate m_τ and less weight to samples below it. Conversely, $\tau < 0.5$ emphasizes lower values. Thus, expectiles interpolate smoothly between the mean ($\tau = 0.5$) and a “high-value-seeking” statistic as $\tau \rightarrow 1$.

Expectile regression can also be extended to learning conditional expectiles:

$$m_\tau(x) = \arg \min_{m(\cdot)} \mathbb{E}_{(x,y) \sim \mathcal{D}} [L^\tau(y - m(x))], \quad (47)$$

which can be optimized efficiently via stochastic gradient descent. This makes expectiles easy to implement in modern machine-learning pipelines, unlike alternative high-order statistics that require specialized solvers.

B. Description of the Experiments

B.1. Boat Navigation

The state $x \in \mathcal{X} = [-3, 2] \times [-2, 2]$ of the 2D Boat system are $x = [x_1, x_2]^T$, where, x_1, x_2 are the x and y coordinates of the boat respectively. We define the step reward at each step, $r(x)$ as:

$$r(x) = C \cdot \left(- \left\| \begin{bmatrix} x_1 \\ x_2 \end{bmatrix} - \begin{bmatrix} x_{g1} \\ x_{g2} \end{bmatrix} \right\| \right) \quad (48)$$

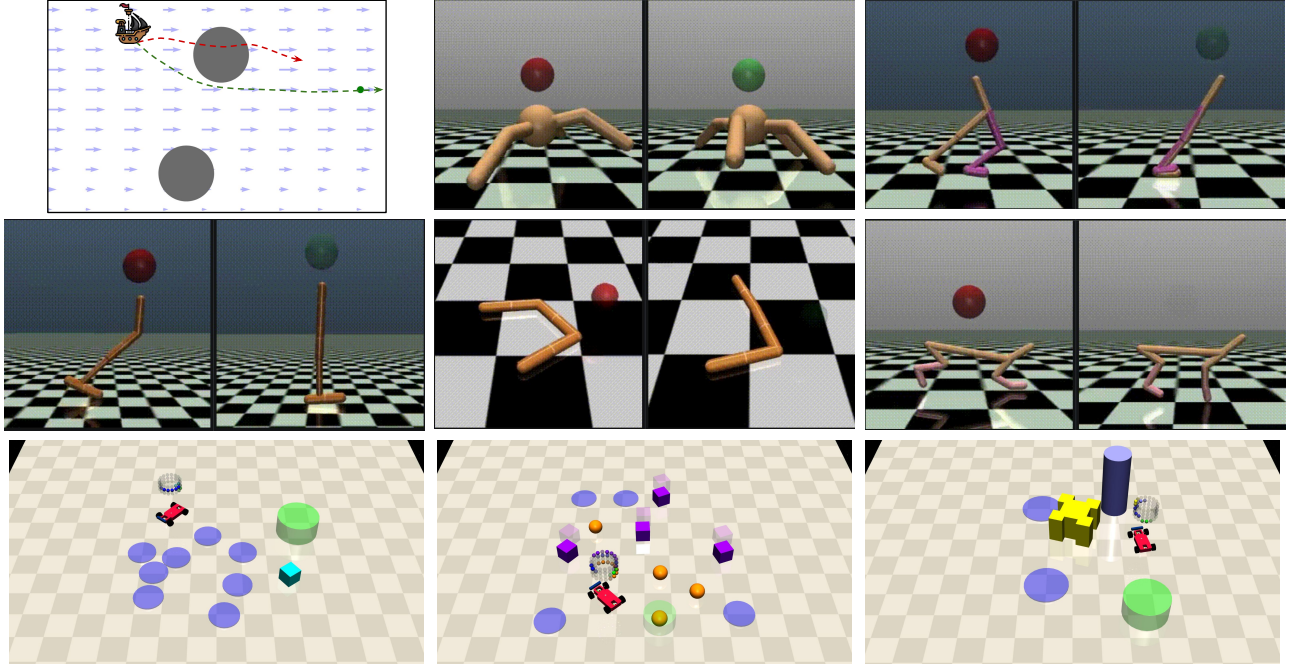


Figure 5. Illustration of all evaluation environments. (Top-Left) environment illustrates Boat Navigation with obstacles and a goal point. (Middle) illustrates SafeVelocity MuJoCo environments with Red sphere denoting unsafe state. (Bottom) depicts the SafeCarNavigation MuJoCo environments with various obstacles and objectives.

where $[x_{g1}, x_{g2}]^T = [0.5, 0.0]^T$ denotes the goal location, and $C = 0.1$. Maximising this reward drives the boat toward the goal. Consequently, the (augmented) dynamics of the 2D Boat system are:

$$\begin{aligned} (x_1)_{t+1} &= (x_1)_t + (a_1 + 2 - 0.5x_2^2) \cdot \Delta t \\ (x_2)_{t+1} &= (x_2)_t + a_2 \cdot \Delta t \\ z_{t+1} &= (z_t - r(x)) / \gamma \end{aligned}$$

where Δt represents discrete time step, a_1, a_2 represent the velocity control action in x_1 and x_2 directions respectively, with $a_1^2 + a_2^2 \leq 1$ and $2 - 0.5x_2^2$ specifies the current drift along the x_1 -axis. The safety constraints are encoded as:

$$\ell(x) := \min(\|x - (-0.5, 0.5)^T\| - 0.4, \|x - (-1.0, -1.2)^T\| - 0.4) \quad (49)$$

where $\ell(x) < 0$ indicates that the boat is inside a obstacle, thereby ensuring that the sub-level set of $\ell(x)$ defines the failure region.

Offline Data Generation. Since this is a custom environment, we construct an offline dataset which can be used to train a safe and performant policy. We sample 2500 initial states uniformly from \mathcal{X} and simulate each trajectory for 400 discrete timesteps with step size $\Delta t = 0.005s$. During data collection, control inputs are drawn uniformly at random from the admissible range, ensuring diverse system trajectories for learning the controller.

B.2. Safety Gymnasium Environments:

To evaluate scalability to higher-dimensional systems we use Safety Gymnasium (Ji et al., 2023). We consider (i) *safe velocity* variants that impose velocity constraints on Gymnasium MuJoCo-v4 agents (HalfCheetah, Hopper, Ant, Walker2D, Swimmer), and (ii) car navigation tasks (CarButton1, CarGoal1, CarPush1) focused on collision avoidance.

The agent receives a scalar cost signal on the basis of its current state at each step. This cost can be framed as a sparse and simple safety function

$$\ell(x) = \begin{cases} 10 & \text{if cost} = 0, \\ -10 & \text{if cost} > 0. \end{cases} \quad (50)$$

since $\ell(x) \geq 0$ corresponds to safe state. This safety value function provides us a sparse signal.

C. Ablation Studies

We conduct a series of ablation studies to isolate and validate the key design choices of our method. The primary testbed for these analyses is the *Safe Boat Navigation* environment, which provides a controlled yet challenging safety-critical setting. Its low-dimensional, 2D structure enables clear visualization and interpretation of policy behavior, while the presence of nonlinear river drift dynamics makes safe navigation nontrivial for existing baselines. While most ablations are centered on the Boat environment, we additionally include select higher-dimensional systems in specific studies to assess robustness and generalization beyond the primary domain. The following subsections detail these analyses.

C.1. Sensitivity to Expectile parameter (τ)

As described in Section 4, we employ a τ -expectile regression objective to learn the auxiliary value function $\hat{V}(x, z)$, which is subsequently used for policy extraction in the SC-MDP setting. When $\tau = 0.5$, the expectile loss reduces to a symmetric mean-squared error objective, yielding an estimate that reflects the average safety and performance induced by the behavior policy. This *behavior-induced* value function is typically overly conservative and fails to emphasize high-quality safe transitions, which is misaligned with the objectives of safety-constrained control.

To study the effect of asymmetric weighting, we compare $\tau = 0.5$ against larger expectile values that place increasing emphasis on the upper tail of the value distribution. Table 1 reports mean episode reward, safety rate, and average episode cost on the Boat Navigation environment for different τ settings.

Table 1. Mean Reward, Safety Rate (%), and Mean Cost reported for Boat Navigation by varying τ in the expectile regression.

τ	0.5 (Behaviour Policy)	0.6	0.7	0.8	0.9
Mean Episode Reward	-485.86 ± 0.74	-486.63 ± 0.88	-492.36 ± 0.21	-496.01 ± 0.58	-496.10 ± 0.37
Safety Rate (%)	88.9 ± 0.23	89.9 ± 0.54	98.9 ± 1.01	99.9 ± 0.18	100.0 ± 0.0
Mean Episode Cost	1.95 ± 0.19	1.14 ± 0.44	0.09 ± 0.03	0.04 ± 0.05	0.0 ± 0.0

We observe that setting $\tau = 0.5$ leads to the lowest safety rate, as the resulting value function underweights safety-critical regions that are infrequently represented in the offline dataset. As τ increases, safety performance improves steadily while reward remains competitive, reflecting stronger alignment with high-value demonstrated actions. Consequently, larger expectile values produce policies that more effectively capture the upper envelope of safe and performant behaviors.

In idealized settings—such as deterministic dynamics with minimal dataset noise, pushing $\tau \rightarrow 1$ concentrates the estimator on the extreme upper tail and can lead to the strongest empirical performance by prioritizing high-value next-state targets. However, this regime is brittle in practice as rare suboptimal actions or stochastic disturbances may generate overly optimistic transitions, causing extreme expectile estimators to overfit spurious outcomes.

Balancing this trade-off, we fix $\tau = 0.9$ in all experiments. This choice substantially up-weights high-value targets while preserving robustness to noise and outliers commonly present in offline datasets.

C.2. Resilience to External Perturbations

We next evaluate the robustness of the recovered policy to perturbations in the executed control action, which indirectly probes sensitivity to errors in the learned auxiliary value function. Specifically, we perturb the selected optimal action a by additive zero-mean Gaussian noise $\mathcal{N}(0, \sigma^2)$, with σ scaled relative to the maximum admissible action magnitude. We consider three perturbation levels—5%, 10%, and 20% of the action bound—and evaluate performance over 100 independent rollouts per setting, using five random seeds. In addition to the Boat Navigation task, we also include two higher-dimensional systems from Safety Gymnasium, namely Safe Velocity HalfCheetah and Ant, to assess robustness beyond the primary environment.

Figure 6 summarizes reward and safety cost trends across perturbation levels. Across all environments, safety costs increase only mildly under small to moderate perturbations, indicating that the learned policies tolerate reasonable inaccuracies in control execution even in safety-critical regimes. While rewards degrade more noticeably at larger perturbation magnitudes,

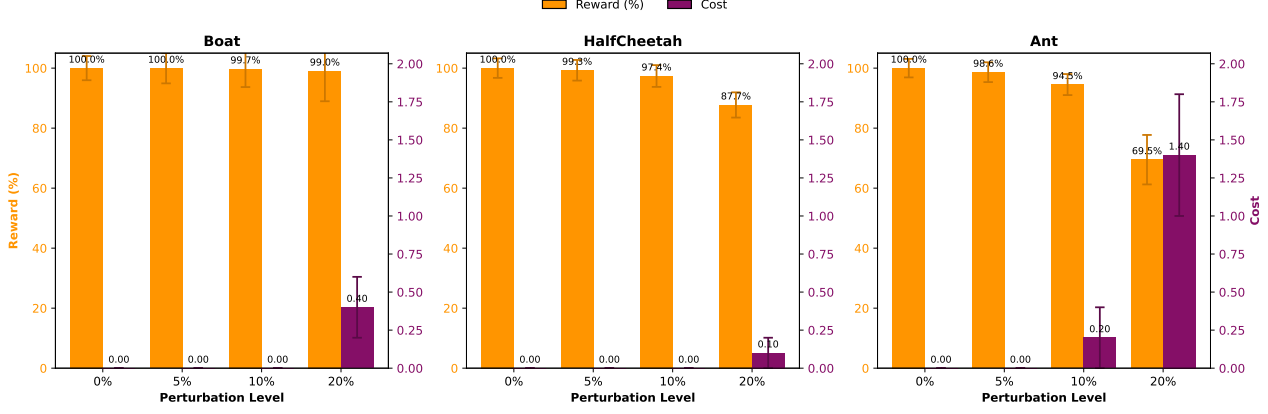


Figure 6. Results for Control under Perturbations. The plots show average reward (%) achieved relative to no perturbations case, at different levels of perturbations (5%, 10% and 20%), and their average absolute cost values respectively.

this degradation becomes significant only under aggressive noise injection. These results suggest that precise action execution improves performance, but our framework retains strong safety-aware behavior and competitive returns under moderate control uncertainty. Future work will investigate uncertainty-aware and robust optimization formulations that explicitly model and mitigate the effects of disturbances.

C.3. Number of Action Samples

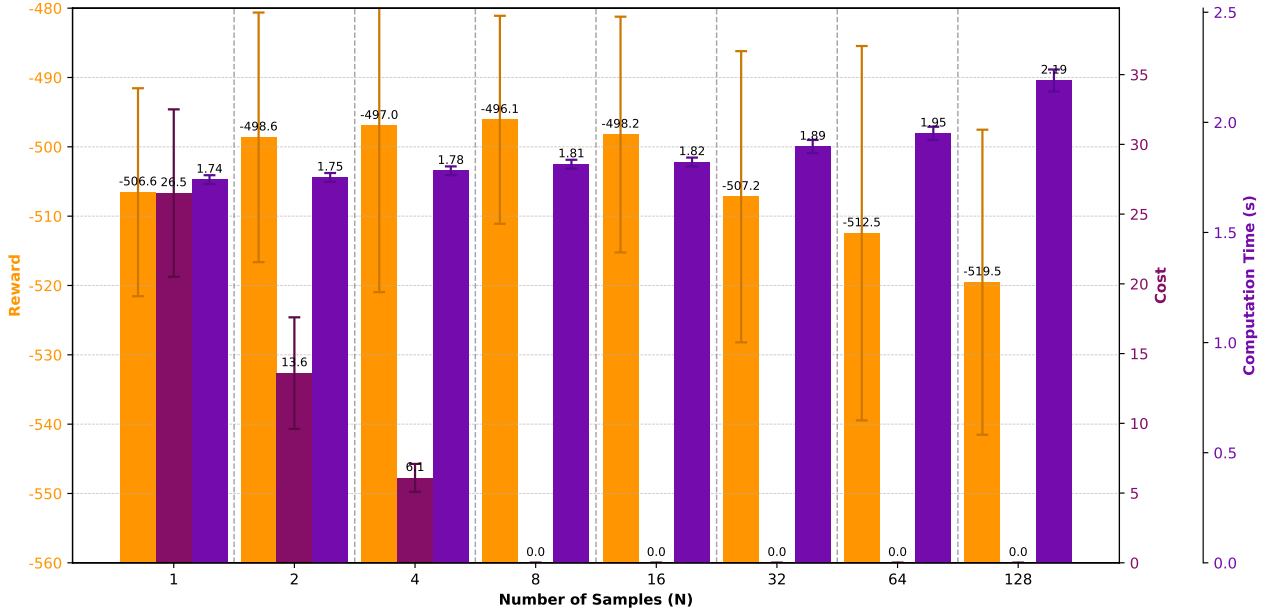


Figure 7. Ablations on number of action samples in Boat Navigation environment

As described in Section 5, our epigraph-guided policy recovery procedure assumes an idealized setting with unlimited model capacity and vanishing approximation error. In practice, such assumptions rarely hold, making direct recovery of the optimal policy challenging. Motivated by prior sample-based guided action selection methods (Park et al., 2025; Hansen-Estruch et al., 2023; Chen et al., 2023), we augment our weighted flow-matching policy with action resampling at inference time. Specifically, we draw N candidate actions from the recovered policy and select the one maximizing the auxiliary value estimate \hat{V} .

To quantify the effect of sampling, we sweep the number of action candidates $N \in \{1, 2, 4, 8, 16, 32, 64, 128\}$ during

evaluation on the Boat Navigation environment. Figure 7 reports reward, safety cost, and inference-time computation as functions of N . We observe that sampling improves performance up to a moderate level, with $N = 8$ achieving the best trade-off: maximal reward, near zero safety violations, and reasonable computational overhead. Beyond this point, additional samples yield diminishing returns while increasing computation time at inference, suggesting that modest sampling suffices for effective policy refinement.

C.4. Effect of the Regularization Constant λ on \hat{V}_θ

We study how the decomposition regularizer (term \mathcal{L}_{reg} in Eq. (15)) affects the learned auxiliary epigraph value \hat{V}_θ by sweeping $\lambda \in \{0.1, 0.25, 0.5, 1.0\}$. Figure 8 visualizes the inferred per-state budget $z^*(x)$ (the largest z such that $\hat{V}_\theta(x, z) \geq 0$) for the Boat Navigation task, and Table 2 summarizes downstream metrics (mean reward, safety rate, mean episode cost).

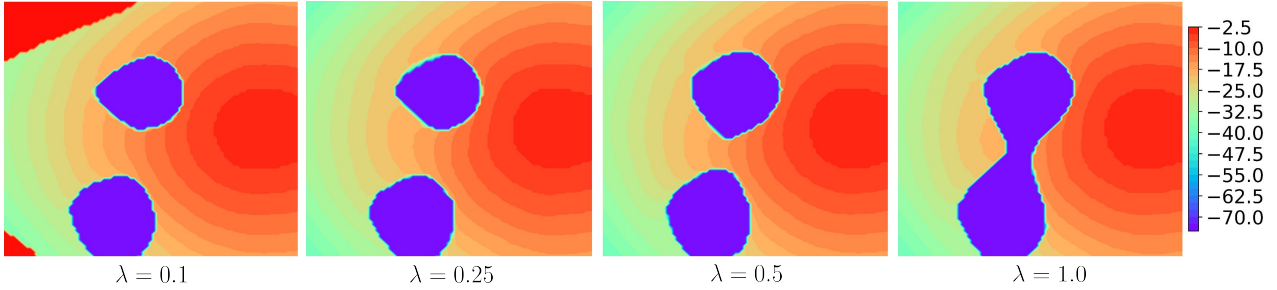


Figure 8. Effect of the regularization weight λ on the inferred epigraph budget. For the Boat Navigation environment, each panel shows the state-wise optimal budget $z^*(x)$ defined by the feasibility condition $\hat{V}_\theta(x, z^*) \geq 0$. As λ increases, the feasible region contracts and $z^*(x)$ becomes more conservative; states shaded in purple correspond to infeasible regions.

The sweep reveals a clear bias–variance trade-off. For small regularization ($\lambda = 0.1$) the decomposition constraint is too weak: \hat{V}_θ exhibits flattening and reduced sensitivity to z , causing inflated estimates of feasibility (larger regions shown feasible) and correspondingly lower safety rates. As λ increases, the decomposition term more strongly enforces the upper bound $\hat{V} \leq \min\{V_r - z, V_s\}$, which reduces uncontrolled drift along the z -axis and enlarges the infeasible region; this improves safety but can reduce returns. In our experiments safety rates approach 100% for $\lambda \geq 0.25$, while very large λ (e.g., 1.0) produces overly conservative feasibility sets and lower mean reward.

Balancing these effects, we select $\lambda = 0.25$ for the main experiments: it sufficiently prevents the z -insensitivity and budget-collapse observed at low regularization, while avoiding the excessive conservatism seen at higher weights. Practitioners should tune λ on a validation set (a useful range is roughly 0.1–0.5) and inspect both sensitivity diagnostics (e.g., variation of \hat{V} across z) and downstream trade-offs between reward and safety when selecting the final value.

Table 2. Mean Reward, Safety Rate (%), and Mean Cost reported for Boat Navigation by varying λ in the regularizer loss term.

λ	0.1	0.25	0.5	1.0
Mean Episode Reward	-483.63 ± 0.31	-496.10 ± 0.37	-510.96 ± 0.58	-616.15 ± 0.48
Safety Rate (%)	87.9 ± 0.42	100 ± 0.0	100 ± 0.0	100.0 ± 0.0
Mean Episode Cost	8.14 ± 0.76	0.0 ± 0.0	0.0 ± 0.0	0.0 ± 0.0

D. Experimental Details

D.1. Experimental Hardware

To keep the evaluation fair and avoid any discriminatory added advantage to any specific experiment, all experiments were conducted on a single system equipped with an 14th Gen Intel Core i9-14900KS CPU, 128GB RAM, and an NVIDIA GeForce RTX 4090 GPU for training and experiment evaluations.

D.2. Network Architecture and Training Details of the Proposed Algorithm

We have compiled and listed down all the hyperparameters that we used to perform our experiments and report the results. These training settings for all the environments are detailed in the Table 3. For the MuJoCo environments, we use the widely accepted DSRL (Liu et al., 2024b) dataset.

Table 3. Hyperparameters for the Algorithm (EpiFlow).

Hyperparameter	Value
Network Architecture	Multi-Layer Perceptron (MLP)
Activation Function	ReLU
Optimizer	Adam optimizer
Learning Rate	3×10^{-4}
Discount Factor (γ)	0.99
No. of Action Candidates (N)	8
Time Step Intervals (FM Policy)	5
Boat Navigation	
Number of Hidden Layers	2
Hidden Layer Size	256 neurons per layer
Dataset Size	1M
Safe Velocity Hopper	
Number of Hidden Layers	3
Hidden Layer Size	256 neurons per layer
Dataset Size	1.32M
Safe Velocity Half-Cheetah	
Number of Hidden Layers	3
Hidden Layer Size	128 neurons per layer
Dataset Size	249K
Safe Velocity Ant	
Number of Hidden Layers	3
Hidden Layer Size	256 neurons per layer
Dataset Size	2.09M
Safe Velocity Walker2D	
Number of Hidden Layers	3
Hidden Layer Size	256 neurons per layer
Dataset Size	2.12M
Safe Velocity Swimmer	
Number of Hidden Layers	3
Hidden Layer Size	256 neurons per layer
Dataset Size	1.68M

During the training, we set the τ for expectile regression in section 4.2 to 0.9. And we use clipped double Q-learning (Fujimoto et al., 2018), taking a minimum of two Q. We update the target Q networks using Exponential Moving Average (EMA) where the weight to the new parameters is set to. Following (Kostrikov et al., 2022), we clip exponential advantages to $(-\infty, 100]$ in feasible part and $(-\infty, 150]$ in infeasible part. For our paper, we used flow matching implementation from IFQL/FQL (Park et al., 2025).

D.3. Hyperparameters for the Baselines

Hyperparameters for the remaining safe offline RL baselines (COptiDICE, BEAR-Lag, BCQ-Lag, CPQ, C2IQL, FISOR) are provided in Table 4. We use the official implementations of BEAR-Lag, BCQ-Lag, CPQ and COptiDICE from (Liu et al., 2024b), of C2IQL from (Liu et al., 2025) and of FISOR from (Zheng et al., 2024), and train all methods on the same DSRL datasets.

Table 4. Detailed Hyperparameters for Baseline Special Networks. (Layers, Units) notation refers to hidden layers and units per layer. All baselines utilize the DSRL dataset standards (Liu et al., 2024b).

Baseline	Network Component	Architecture Specification
C2IQL (Liu et al., 2025)	Actor / Critic / Value Nets	MLP, (256, 2)
	Cost Reconstruction Model	MLP, (5 layers, 512 units each)
	Reward / Cost Advantage	MLP, (256, 2)
BCQ-Lag (Lag. dual of (Fujimoto et al., 2019))	VAE (Encoder/Decoder)	MLP, (750, 2), Latent Dim: $2 \times$ Action Dim
	Perturbation Model ξ	MLP, (400, 2)
	Double Q-Critics	MLP, (400, 2)
CPQ (Xu et al., 2022)	Actor (Policy) Net	MLP, (256, 2)
	Constraint-Penalized Q	Ensemble DoubleQCritic, (256, 2)
	Cost Critic Net	MLP, (256, 2)
FISOR (Zheng et al., 2024)	Diffusion Denoiser (Actor)	DiffusionDenoiserMLP, (256, 2)
	Feasibility Classifier	MLP, (256, 2), Sigmoid Output
	Energy/Value Guidance	MLP, (256, 2)
COptiDICE (Lee et al., 2022)	Dual / ν Network	DualNet (Value-like), (256, 2)
	Actor (Extraction) Net	MLP, (256, 2)
BEAR-Lag (Lag. dual of (Kumar et al., 2019))	VAE (Support Model)	MLP, (750, 2)
	Actor (Policy) Net	SquashedGaussianMLPActor, (256, 2)
	Cost / Reward Critics	MLP, (256, 2)